

Dressing Plasmons in Particle-in-Cavity Architectures

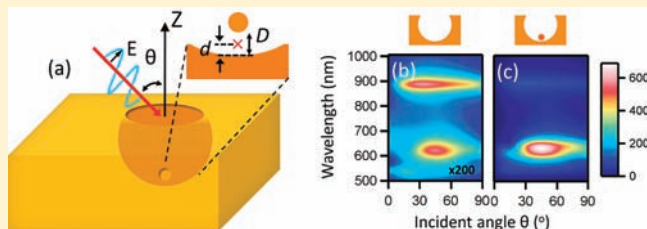
Fu Min Huang,^{*,†} Dean Wilding,[†] Jonathon D. Speed,[‡] Andrea E. Russell,[‡] Philip N. Bartlett,[‡] and Jeremy J. Baumberg[†]

[†]Nanophotonics Centre, Cavendish Laboratory, University of Cambridge, J J Thomson Avenue, Cambridge, CB3 0HE, U.K.

[‡]Department of Chemistry, University of Southampton, Southampton, SO17 1BJ, U.K.

ABSTRACT: Placing metallic nanoparticles inside cavities, rather than in dimers, greatly improves their plasmonic response. Such particle-in-cavity (PIC) hybrid architectures are shown to produce extremely strong field enhancement at the particle–cavity junctions, arising from the cascaded focusing of large optical cross sections into small gaps. These simply constructed PIC structures produce the strongest field enhancement for coupled nanoparticles, up to 90% stronger than for a dimer. The coupling is found to follow a universal power law with particle–surface separation, both for field enhancements and resonant wavelength shifts. Significantly enhanced Raman signals are experimentally observed for molecules adsorbed in such PIC structures, in quantitative agreement with theoretical calculations. PIC architectures may have important implications in many applications, such as reliable single molecule sensing and light harvesting in plasmonic photovoltaic devices.

KEYWORDS: Surface plasmon, surface-enhanced Raman scattering, particle-in-cavity, power-law dependence, cascaded field enhancement, nanoparticle dimer



The optical properties of metallic nanostructures with gaps at nanometer scales have received considerable research interest in the past decade. At such small gaps, strong electromagnetic coupling leads to many interesting optical phenomena, such as tight light confinement at the junctions of nanostructures. These enhanced local optical fields have many important applications, such as molecular sensing,¹ light harvesting,² and subwavelength imaging.³ Much effort has been devoted to finding geometries exhibiting strong optical effects which are fabricatable with high reliability. Widely studied structures include nanoparticle dimers,^{4–6} chains,⁷ arrays,^{8,9} voids,^{10–12} and nanoparticles on flat surfaces.^{15,16} However, little is known about configurations in which individual particles are coupled to an extended metallic nanostructure such as a cavity, with only brief theoretical studies of nanoparticles atop cavities,¹⁷ and optical trapping of nanorods inside nanovoids,¹⁸ both as yet unrealized.

Here we provide both theoretical and experimental studies of the plasmonic properties of metallic nanoparticles inside metallic cavities. Such metallic cavities support multiple cavity–plasmon modes^{11,12} which confine light very strongly inside the void. This allows them to induce the strong-coupling “normal-mode” regime and, more significantly, cascaded optical field enhancement when particles are introduced inside them. Cascaded electromagnetic field enhancements have been demonstrated on various geometries,^{13,14} generating extremely strong field enhancement.

Theoretical simulations indicate that particle-in-cavity (PIC) architectures produce extremely strong field enhancements at the particle–cavity junctions when one of the cavity modes is resonant with the cavity-dressed nanoparticle mode. These results are compared to nanoparticles near any general object

of arbitrary radius of curvature, including flat surfaces or other spherical particles. The PIC structures produce the strongest field enhancement (throughout the paper, the “field enhancement” refers to the local electric field enhancement at peak wavelength) among these geometries, up to 90% stronger than that produced by a particle dimer excited under optimal conditions, and therefore they can be exploited for single molecule sensing.^{19–21} As a nanoparticle is brought close to the surface of a nanostructure, it induces strong optical fields in the gap as well as red-shifting the resonant wavelength. Both the resonant wavelength shift and the field enhancement exhibit a power law dependence on the particle–nanostructure gaps, an effect closely related to the Casimir effect²² and not well understood. This power law dependency is universal, applying to all the various geometries at all size scales. Experimentally we construct such PIC dimers and observe significantly enhanced surface-enhanced Raman signals (SERS) of adsorbed molecules in quantitative agreement with theoretical calculations.

The geometry of the investigated architecture is schematically shown in Figure 1. The cavities used are truncated spherical nanovoids of radius 100–500 nm; however the principles outlined here apply to any general voidlike cavity geometry. Gold truncated spherical nanovoids with radius R and height h are illuminated with p-polarized light at an incident angle θ with respect to the vertical z axis. Plasmon modes in such voids have been fabricated and well-studied over the past few years.^{10–12} Throughout this paper the void height is fixed to be $h = 1.5R$,

Received: December 3, 2010

Revised: January 7, 2011

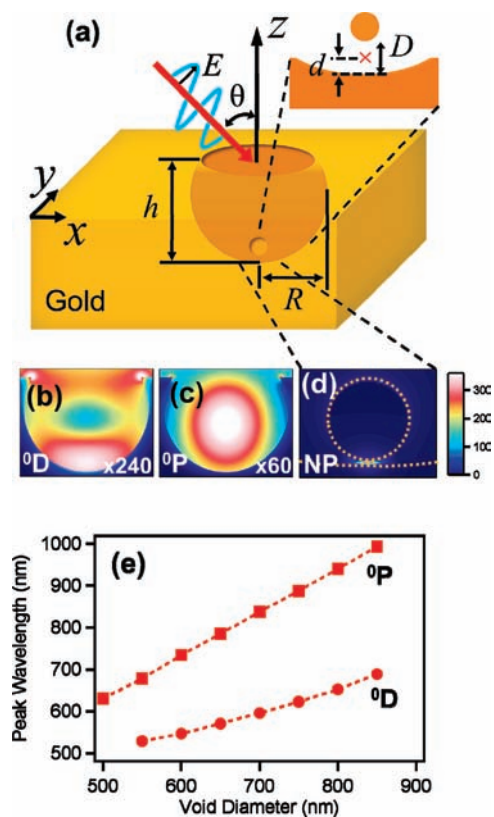


Figure 1. (a) Schematic diagram of particle-in-cavity geometry. (b–d) Calculated field distributions of (b) 0D mode and (c) 0P mode of an empty 600 nm Au nanovoid, and of the NP mode with a 60 nm particle inside it separated $D = 1$ nm above the bottom (dashed lines indicate the boundary of the nanoparticle and void). Color scales in (b, c) multiplied by factors of 240 and 60, respectively. (e) Resonant wavelengths of void modes as a function of void size.

which is optimal for SERS. We investigate the field enhancement at a fixed point (red \times , Figure 1) spaced $d = 0.25$ nm above the inner surface of the nanovoids (or equivalently 0.25 nm above the surface of each nanostructure). When a nanoparticle is very close to a surface, the field within the gap (of width D) is almost uniform.²³ Hence we choose this fixed point (\times) for convenience to compare effects of different particle–void separations, particularly down to $D < 1$ nm. Excitation by p-polarized light is used since it induces much stronger plasmonic effects than s polarization. While nanoparticle sizes of fixed diameter 60 nm are reported here (unless explicitly stated), similar results are obtained for nanoparticles of diameters from 10 to 100 nm. All simulations are calculated using the boundary element method, which is particularly efficient in solving electromagnetic problems in such axial-symmetric systems.^{24,25} The dielectric constants of materials are taken from Johnson and Christy.²⁶

Metallic cavities such as nanovoids^{11,12} have interesting optical properties in their own right with applications such as SERS²⁷ and omnidirectional optical absorption,²⁸ which can be exploited for enhancing photovoltaic efficiencies. Nanovoids possess multiple plasmonic modes that can be specifically tailored by varying the void geometry or incident conditions, such as the incident angles and polarizations of light.^{11,12} The two dominant plasmonic modes here are the so-called 0D mode and 0P mode,¹² which have typical field distributions inside nanovoids as shown in parts b and c of Figure 1 (mapping $|E|$ in the yz plane across the

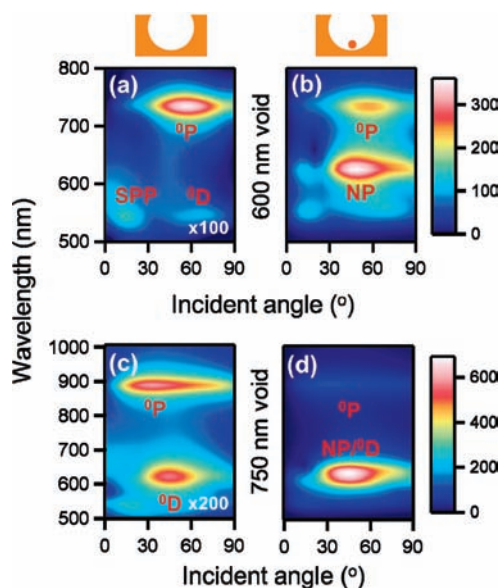


Figure 2. Calculated field enhancement spectral maps of (a, b) Au void of diameter 600 nm and (c, d) Au nanovoid of diameter 750 nm: (a, c) empty voids, (b, d) with a 60 nm Au sphere 1 nm away from the void surface. Note: color scales of (a) and (c) are multiplied by factors of 100 and 200, respectively.

void center). The 0D mode confines light near the bottom of the void, while the 0P mode concentrates light near the center of the void. These optical modes are tunable with void size, scaling almost linearly with void size at longer wavelengths (Figure 1e). This feature provides straightforward tunability of optical properties, which is crucial for many applications.

The calculated spectral map of field enhancement at point \times for an empty Au void of 600 nm diameter at different incident angles shows several optical modes (Figure 2a). The long- λ resonance around 740 nm is optimally excited with an incident angle of 55° and is the 0P mode (field distribution as in Figure 1c). The mode peaked at 545 nm optimally excited at 60° incidence is the 0D mode (field distribution in Figure 1b). Both the 0P and 0D modes have field polarizations along the z axis. On the left side of the 0D mode in Figure 2a is another mode (denoted “SPP”) with peak wavelength close to that of the 0D mode. However, this mode does not shift with void size and does not appear on voids of other materials. This mode is the bulk plasmon of gold, which is usually unseen on flat surfaces but can be excited on curved geometries such as the voids discussed here. The presence of this mode perturbs the 0D mode, which usually has a more symmetric distribution pattern (as seen in Figure 2c for a 750 nm void).

For an empty void the 0P mode produces the strongest field (Figure 2a), concentrating light near the center of the void (Figure 1c). However when a nanoparticle is introduced into this nanovoid, the situation changes dramatically. The corresponding field enhancement spectral map at the same point (Figure 2b) with a spherical Au nanoparticle (diameter 60 nm) placed at a position $D = 1$ nm above the void bottom surface shows that all optical modes are strongly enhanced (note the color scale of Figure 2a has to be multiplied by a factor of 100). In addition there is a strikingly strong extra optical mode appearing around 627 nm, which is optimally excited at 50° incidence. Unlike the 0D and 0P modes, the resonant wavelength of this mode is almost independent of void size but sensitively dependent on the distance between nanoparticle and void. For reasons which will

become clear, this mode is due to the coupling between the nanoparticle and its image and hereafter denoted the “NP” mode. The NP mode produces high field enhancements of >350 , confined at the particle–void junction (Figure 1d). For comparison, without the presence of the nanoparticle, the maximum enhancement at the same λ and spatial location is only 3 for the ^0D mode. This strong field enhancement can be further enhanced when one of the void modes is tuned to be simultaneously resonant with the NP mode, which is simple to achieve since the void modes readily tune with void size (Figure 1e). For a 60 nm Au nanoparticle and 1 nm gap, the NP mode is resonant with the ^0D mode of a 750 nm Au void. The calculated spectral map of a 750 nm Au void (Figure 2c) clearly shows a ^0P mode at 890 nm and a ^0D mode at 625 nm. When a 60 nm nanoparticle is placed 1 nm away from the void surface, the local fields are strongly enhanced for all optical modes, as clearly seen in Figure 2d (note the color scale in Figure 2c had to be multiplied by a factor of 200). However as the ^0D mode is now resonant with the NP mode, this produces an extremely strong hybrid NP/ ^0D mode, dominating all modes in the map. The hybrid NP/ ^0D mode is so strong (maximum enhancement 730 at 630 nm) that the ^0P mode is only weakly visible in the image, despite also having been significantly enhanced.

To further investigate the particle–cavity coupling effects, we calculate the spectra of field enhancement of the PIC structure with a 60 nm Au nanoparticle at different distances above the inner surface of a 750 nm Au void (with incident angle fixed at 45° , which is optimal to excite the hybrid NP/ ^0D mode). The spectra (Figure 3a) clearly show three optical modes which get stronger as the nanoparticle moves closer to the nanovoid. This should be compared to the field enhancement spectra of an empty void (black curve, Figure 3a, multiplied by a factor of 20). Despite the strong effect of the ^0P on the localized plasmons of the nanoparticle, the resonant wavelength of the ^0P mode itself is almost unchanged by the nanoparticle. This is because the nanoparticle is small compared to the cavity plasmon mode volume and near the bottom of the void, far away from the center of the ^0P mode (Figure 1c), thus has little influence on the mode frequency. At close distances the ^0D mode and the NP mode couple to each other, producing extremely strong field enhancement. All spectra between 500 and 800 nm can be well fit with two Lorentzian peaks, and the results produce an anticrossing behavior (Figure 3b), showing a Rabi splitting of 20 nm, indicating that the ^0D mode and NP mode attain the normal-mode regime in which the splitting exceeds their line width.

To quantify the improvements from negative curvature coupling compared to dimers, we characterize the coupling of Au nanoparticles to different surface curvatures, including dimers, flat disks, and nanoparticles of different sizes. Figure 4 shows the calculated maximum field enhancement of a 60 nm Au sphere near various Au geometries, for fixed separation of $D = 1$ nm. The field enhancements are optimized for the input polarization and incident angle of light. For instance the dimer system is optimally excited when the incident light is illuminated perpendicular to the dimer axis, with the polarization parallel to the dimer axis (inset, Figure 5a); the particle–disk system is optimally excited with p-polarized light incident at 70° to the vertical axis normal to the disk surface; the particle–void geometry is best excited at 45° . The horizontal axis of Figure 4 is the inverse radius of curvature of each geometry (corresponding to the scaled angular momentum¹⁰), including voids of 300, 600, and 750 nm diameter, a flat disk (750 nm diameter), and nanoparticles of 750, 300, and

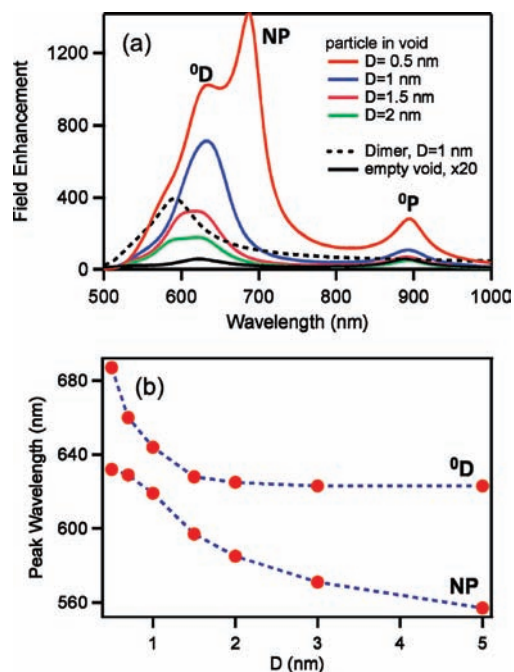


Figure 3. (a) Calculated field enhancement spectra of a 60 nm Au sphere inside a 750 nm Au nanovoid, at various particle–void separations D , 60 nm Au sphere dimer (dashed line), and empty void (solid black). (b) Anticrossing behavior of the ^0D and NP modes.

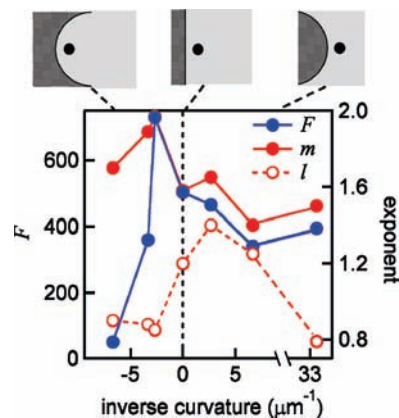


Figure 4. Calculated field enhancement (blue) of a 60 nm Au sphere spaced 1 nm above various radius of curvature structures, and extracted exponents (red) of field enhancement (●) and resonant wavelength shift (○). The horizontal axis is the inverse of the radius of curvature. From left to right: 300 nm, 600 nm, and 750 nm nanovoids, 750 nm flat disk, and 750 nm, 300 and 60 nm (dimer) spheres.

60 nm dimers. It is clear that the particle-in-cavity geometry produces the strongest field enhancement, when the cavity mode is resonant with the NP mode (750 nm void), which is about 90% stronger than that of the dimer (black dashed line, Figure 3a). The reason is that metallic cavities act as effective light harvesters, resonantly concentrating light (such as at the ^0D mode) near the bottom of void surface, therefore significantly enhancing the coupling between particles and image particles inside voids.

It is known that dipole coupling between nanoparticles⁶ or nanoparticles near flat surfaces^{15,16} red shifts the resonant wavelengths. Similarly Figure 3 shows clear red-shifted peak wavelengths as the particle–void gap decreases. To clearly resolve this

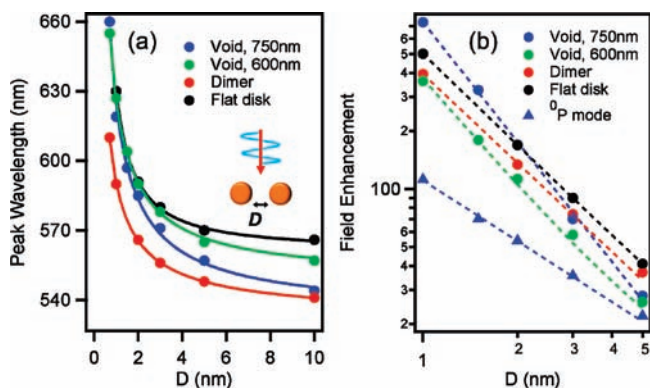


Figure 5. (a) Resonant wavelengths and (b) field enhancements of the NP modes of a 60 nm Au sphere as a function of its separation D from the surface of various structures, with power law fits (lines). Inset in (a): optimal excitation of dimer.

effect, the peak wavelengths of each NP mode are systematically plotted against particle–surface gap D , for the various geometries (Figure 5a). Contrary to the frequently assumed exponential dependence, we find that the resonant wavelengths, λ , are properly fit with power laws: $\lambda = cD^{-l} + \lambda_0$, where c , λ_0 , and l are fitting parameters. The field enhancements, F , also follow a power law with the particle–surface separation (Figure 5b). As the fields in the gaps are so much stronger than that without nanoparticles, the constant part of the power law function is negligible in this range and $F = c'D^{-m}$, clearly indicated by the straight lines on a log plot of F (Figure 5b). This power law dependence is universal, applying to every geometry, such as particle–void, particle–particle, and particle–flat surfaces. We have examined these geometries for a wide range of sizes, for voids ranging from 300 to 1000 nm, and for dimers ranging from 20 to 250 nm, and in all cases they follow power laws extremely well.

To the best of our knowledge, this universal power law dependence for both the resonant wavelength shift and the field enhancement has not been clearly demonstrated before. Like many authors, Jain et al. report an empirical exponential dependence of resonant wavelengths on interparticle gaps of dimers.⁶ Here we generalize to various geometries with a wide range of sizes and shapes and conclude that the power-law dependence for both resonant wavelength shift and field enhancement are universal in nanophotonic coupling at short-range. While Maxwell's equations have been analytically solved in a few limited cases,²⁹ electromagnetic problems of complicated geometries have to be tackled by numerical simulations or with severe approximations.

We extract the power law exponents from the simulations (Figure 5b) and find the field enhancement exponent m varies between 2.0 and 1.5, depending on the radius of curvature of the coupling structure. This exponent is well correlated with absolute field enhancement, with the highest exponents for the strongest field enhancement (Figure 4). Recently it was noted that a rectangular particle above a flat surface also shows a power law for the field enhancement at short separations with exponent 1.5, in good agreement with Figure 4.³⁰ The exponents of resonant wavelength shift are also extracted from our simulations and are generally smaller than those of field enhancement (Figure 4). The simultaneous power-law dependence of both resonant wavelength shift, $\Delta\lambda$, and field enhancement, F , connects them in an empirical relationship

$$\Delta\lambda \propto F^{l/m} \quad (1)$$

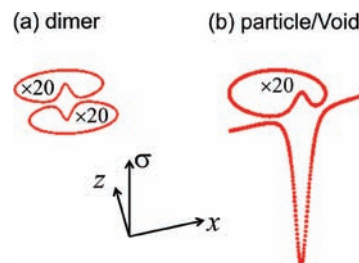


Figure 6. Calculated surface charge density for geometries of (a) dimer and (b) nanoparticle inside a void, excited at optimal conditions. The charge densities on nanoparticles are multiplied by a factor of 20.

This relationship is useful for designing and analyzing a wide range of plasmonic devices, with the exponent $0 < l/m < 1$ minimized for the highest enhancement geometries. For positive radius of curvature, $l/m \approx 0.8$ so that the wavelength shifts almost linearly with the field enhancement. However for the void structures with negative curvature, $l/m \approx 0.5$ so that the wavelength shifts significantly less. This behavior comes from the stronger plasmon modes in void geometries which are less affected by the coupling to the particle, but which provide large cross section field enhancements.

The power-law dependence has a deep connection with that of the Casimir effect between metal plates²² which arises from the zero-point-energy-induced fluctuation forces summed over the classical optical density of states and originates in the retarded Van der Waal's interaction between nearby metals including the plasmonic and photonic contributions.^{31,32} For gaps between a sphere and flat plate which are narrow compared to the radius of curvature and wavelength, the Casimir interaction energy scales as D^{-3} for perfect metals, which changes to $D^{-2.5}$ for real Au.³³ In the approximation that the lateral extent of the gap plasmons scales as $(RD)^{1/2}$, this implies that the field enhancement scales as $D^{-1.75}$ for real Au, similar to the scaling found in our simulations (Figure 5b). These scalings have been found to be very sensitive to the precise metal and geometry involved.^{34,35} While analytic solutions are not easy to obtain, the universal behaviors seen here should be amenable to further theoretical investigation.

It is clear from the power scaling of Figure 5 that the NP modes of nanoparticles inside nanovoids have similar qualitative behaviors to that of dimers or particles near flat surfaces. This arises from their similar origin in the coupling of nanoparticles and their images.^{15,16} However the modified geometry causes some significant differences, such as greater red shifts for resonant wavelengths of nanoparticles inside nanovoids compared to dimers at the same separation. Simulations indicate that more charge accumulates at the junctions in the particle–cavity systems than in dimer systems (Figure 6) accounting for the larger wavelength shifts at close distances. This greatly enhanced charge contribution is due to the large effective cross section of the resonant cavity plasmons.

The presence of a nanoparticle also strongly enhances the spectrally nearby void mode (Figure 3a), even though it is not resonant with the NP mode. The enhancement of the 0P mode field as the particle approaches the void (Figure 4, triangles) also follows the power-law dependence. This exemplifies a key advantage of particle–cavity coupling since strong field enhancements are excited at all the different cavity modes spanning a wide range of wavelengths, which is extremely useful for many applications. Furthermore, this coupling effect is not restricted

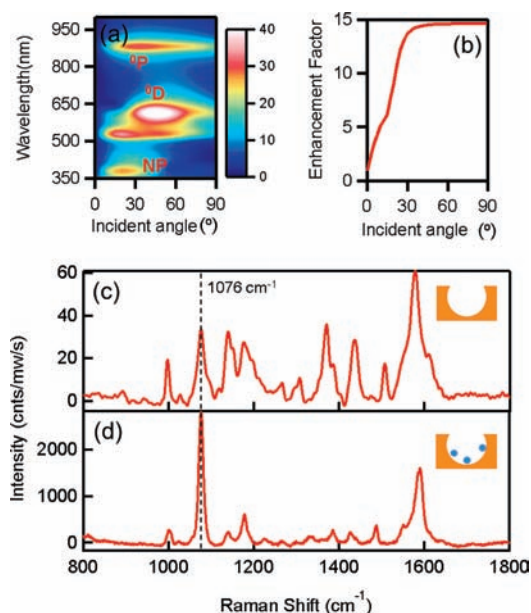


Figure 7. (a) Calculated field enhancement spectral map of a 20 nm Ag sphere inside a 750 nm Au void, at a distance of $D = 1$ nm. (b) The ratio between the field enhancement with and without the Ag nanoparticle. (c, d) Measured SERS spectra of monolayer of 4-aminothiophenol adsorbed in a 600 nm Au void, without (c) and with (d) 20 nm Ag nanoparticles. Excitation laser 633 nm.

to particles and cavities of the same material, and particles and cavities of Au and Ag also induce strong field enhancement. For example the field enhancement spectra (Figure 7a) of a 20 nm Ag spherical particle 1 nm above the bottom of a 750 nm Au void show similar effects to those described above. Compared to the empty void (Figure 2c), it is obvious that both the 0D mode and the 0P mode are strongly enhanced, even though they are not resonant with the NP mode (at 380 nm, as labeled).

To demonstrate the utility of PIC architectures, we use these 20 nm Ag nanoparticles in Au voids for SERS of self-assembled molecular monolayers (SAMs) which allow quantification of the signal. Bare Au voids have been shown already for many years to be highly reliable SERS substrates. The measured SERS spectrum for 633 nm excitation of a 4-aminothiophenol SAM adsorbed on a 600 nm Au nanovoid (height $h = 1.5R$) and then washed to a monolayer, is shown in Figure 7c. Note the void modes are red-shifted 15% compared to simulations due to the perturbation from connecting holes between the voids,¹¹ so that 600 nm voids have resonances matching the 750 nm simulations above. When the substrates are soaked in a solution of 20 nm Ag nanoparticle for 2 h and then washed, a fraction $f = 10\%$ of the Au void surface becomes coated with well-separated Ag nanoparticles (as measured using surface electrochemistry and SEMs). The subsequent Raman spectra remain uniform across the substrate but show a strong additional SERS enhancement (Figure 7d). All Raman modes are enhanced with the strongest lines being those vibrations particularly susceptible to electromagnetic enhancements.^{36,37} In particular the Raman ring mode at 1076 cm^{-1} is 85 times stronger after Ag nanoparticles are added (with enhancements from other vibrations modified by polarization and chemical effects). This effect is predicted by the calculated field enhancement ratio (Figure 7b) comparing a 750 nm Au nanovoid both *with* and *without* a 20 nm Ag nanoparticle inside, excited with a p-polarized 633 nm laser. The presence of

the Ag nanoparticle enhances by 14 times the local field in the particle–void gap beyond 40° incident angles. Since the active area beneath the Ag nanoparticles (which are spaced 1 nm by the SAM above the void) is set by the 10 nm spatial extent of the gap field (Figure 1d), the actual SERS enhancement observed is $85(60\text{ nm}/10\text{ nm})^2/f = 3.1 \times 10^4$, which corresponds to a field enhancement of 13.2 in good agreement with the simulations. We note however that by tuning the modes, nanoparticles, and laser wavelengths appropriately, SERS enhancements of $>10^{10}$ are in prospect given its dependence on the fourth power of the optical field.³⁸ We also note that while the simulations employing cylindrical symmetry cannot give an exact account of the geometry in these experiments, the principle that nanoparticles enhance the resonant cavity plasmonic fields at the void plasmon location at which they are situated supports the interpretation here.

In summary the plasmonic ball-and-socket morphology of particle-in-cavity architectures offers highly controllable and strong coupling between nanoparticles and plasmonic cavities. These metallic voidlike cavities act effectively as light harvesters, with the nanoparticles further focusing the optical fields and concentrating light near the surface of metallic nanovoids, which enhances the strong coupling between nanoparticles and their image inside the metal. Such negative curvature nanostructures are shown to provide the most enhanced coupling of all architectures that can couple to nanoparticles. Producing well controlled nanometer-scale gaps is feasible through molecular SAMs (as here), through controlled dielectric coating for instance using atomic layer deposition (ALD), and through mechanoelastic tuning.³⁹ With the straightforwardly fabricatable geometries studied here (60 nm Au spheres 1 nm away from Au voids), field enhancements up to 730-fold are found, thus able to produce enormous (3×10^{11})-fold enhancements of Raman signals. The simple nature of the particle-in-cavity assembly and current results suggest the reliability of these SERS substrates in contrast to existing problems with hot spots for single-particle SERS and enhanced fluorescence. The strong field enhancement can be further improved by optimizing the nanoparticle (size and shape) and void geometries (such as the void height, which is fixed at $h = 1.5R$ in the work here). Therefore PIC structures have great potential for single molecule sensing.^{19–21} We also demonstrate that both the resonant wavelength shift and field enhancement follow universal power-law dependences on the particle–surface gaps. Finally, we experimentally demonstrate strongly enhanced and reliable Raman signals of monolayers of 4-aminothiophenol adsorbed in Ag–Au PIC nanovoids, well matching quantitatively theoretical predictions. Besides the strongly enhanced local fields, PIC structures have many other advantages making them appealing plasmonic devices, including their ease of mass fabrication, wide and simple tunability of optical properties, and reliable control of particle–cavity separations. Compared to linking solution-based nanoparticles together or direct fabrication, dimers in which one nanostructure component is firmly anchored to a substrate deliver much improved control and reliability. As such, PIC nanostructures form novel architectures with important implications in many applications, such as single molecule sensing and light harvesting in plasmonic photovoltaic devices.

■ AUTHOR INFORMATION

Corresponding Author

*E-mail: fh281@cam.ac.uk.

■ ACKNOWLEDGMENT

This work is supported by EPSRC Grants EP/G060649/1 and EP/F059396/1.

■ REFERENCES

- (1) Anker, J. N.; Hall, W. P.; Lyandres, O.; Shah, N. C.; Zhao, J.; Van Duyne, R. P. *Nat. Mater.* **2009**, *7*, 442–453.
- (2) Atwater, H. A.; Polman, A. *Nat. Mater.* **2010**, *9*, 205–213.
- (3) Huang, F. H.; Festy, F.; Richards, D. *Appl. Phys. Lett.* **2005**, *87*, No. 183101.
- (4) Lassiter, J. B.; Aizpurua, J.; Hernandez, L. I.; Brandl, D. W.; Romero, I.; Lal, S.; Hafner, J. H.; Nordlander, P.; Halas, N. J. *Nano Lett.* **2008**, *8*, 1212–1218.
- (5) Reinhard, B. M.; Siu, M.; Agarwal, H.; Alivisatos, A. H.; Liphardt, J. *Nano Lett.* **2005**, *5*, 2246–2252.
- (6) Jain, P. K.; Huang, W.; El-Sayed, M. A. *Nano Lett.* **2007**, *7*, 2080–2088.
- (7) Brongersma, M. L.; Hartman, J. W.; Atwater, H. A. *Phys. Rev. B* **2000**, *62*, No. R16356.
- (8) Kabashin, A. V.; Evans, P.; Pastkovsky, S.; Hendren, W.; Wurtz, G. A.; Atkinson, R.; Pollard, R.; Podolskiy, V. A.; Zayats, A. V. *Nat. Mater.* **2009**, *8*, 867–871.
- (9) Li, J. F.; Huang, Y. F.; Ding, Y.; et al. *Nature* **2010**, *464*, 392–395.
- (10) Netti, M. C.; Coyle, S.; Baumberg, J. J.; Ghanem, M. A.; Birkin, P. R.; Bartlett, P. N.; Whittaker, D. M. *Adv. Mater.* **2001**, *13*, 1368–1370.
- (11) Kelf, T. A.; Sugawara, Y.; Cole, R. M.; Baumberg, J. J.; Abdelsalam, M. E.; Cintra, S.; Mahajan, S.; Russell, A. E.; Bartlett, P. N. *Phys. Rev. B* **2006**, *74*, No. 245415.
- (12) Cole, R. M.; Baumberg, J. J.; Garcia de Abajo, F. J.; Mahajan, S.; Abdelsalam, M.; Bartlett, P. N. *Nano Lett.* **2007**, *7*, 2094–2100.
- (13) Li, K.; Stockman, M. I.; Bergman, D. J. *Phys. Rev. Lett.* **2003**, *91*, No. 227402.
- (14) Kravets, V. G.; Zorinians, G.; Burrows, C. P.; Schedin, F.; Casiraghi, C.; Klar, P.; Geim, A. K.; Barnes, W. L.; Grigorenko, A. N. *Phys. Rev. Lett.* **2010**, *105*, No. 246806.
- (15) Knight, M. W.; Wu, Y.; Lassiter, J. B.; Nordlander, P.; Halas, N. J. *Nano Lett.* **2009**, *9*, 2188–2192.
- (16) Hill, R. T.; Mock, J. J.; Urzhumov, Y.; Sebba, D. S.; Oldenburg, S. J.; Chen, S.-Y.; Lazarides, A. A.; Chilkoti, A.; Smith, D. R. *Nano Lett.* **2010**, *10*, 4150–4154.
- (17) Ross, B. M.; Lee, L. P. *Opt. Express* **2009**, *17*, 6860–6866.
- (18) Sainidou, R.; Garcia de Abajo, F. J. *Phys. Rev. Lett.* **2008**, *101*, No. 136802.
- (19) Kinkhabawala, A.; Yu, Z.; Fan, S.; Avlasevich, Y.; Mullen, K.; Moerner, W. E. *Nat. Photonics* **2009**, *3*, 654–657.
- (20) Lim, D. K.; Jeon, K. S.; Kim, H. M.; Nam, J. M.; Suh, Y. D. *Nat. Mater.* **2010**, *9*, 60–67.
- (21) Shuming, N.; Steven, R. E. *Science* **1997**, *275*, 1102–1106.
- (22) Casimir, H. B. G. *Proc. K. Ned. Akad. Wet.* **1948**, *51*, 793.
- (23) Aravind, P. K.; Metiu, H. *Surf. Sci.* **1983**, *124*, 506–528.
- (24) Xu, H.; Aizpurua, J.; Kall, M.; Apell, P. *Phys. Rev. E* **2000**, *62*, 4318.
- (25) Garcia de Abajo, F. J.; Howie, A. *Phys. Rev. B* **2002**, *65*, No. 115418.
- (26) Johnson, P. B.; Christy, R. W. *Phys. Rev. B* **1972**, *6*, 4370–4379.
- (27) Cole, R. M.; Mahajan, S.; Baumberg, J. J. *Opt. Express* **2009**, *17*, 13298–13308.
- (28) Teperik, T. V.; Garcia de Abajo, F. J.; Borisov, A. G.; Abdelsalam, M.; Bartlett, P. N.; Sugawara, Y.; Baumberg, J. J. *Nat. Photonics* **2008**, *2*, 299–301.
- (29) Jackson, J. D. *Classical Electrodynamics*, 2nd ed.; Wiley: New York, 1975.
- (30) Leveque, G.; Martin, O. J. F. *Opt. Express* **2006**, *14*, 9971–9981.
- (31) Bressi, G.; Carugno, G.; Onofrio, R.; Ruoso, G. *Phys. Rev. Lett.* **2002**, *88*, No. 041804.
- (32) Intravaia, F.; Lambrecht, A. *Phys. Rev. Lett.* **2005**, *94*, No. 110404.
- (33) Palasantzas, G.; van Zwol, P. J.; De Hosson, J. Th. M. *Appl. Phys. Lett.* **2008**, *93*, No. 121912.
- (34) Klimov, V. V.; Lambrecht, A. *Plasmonics* **2009**, *4*, 31.
- (35) Klimchitskaya, G. L.; Mohideen, U.; Mostepanenko, V. M. *Rev. Mod. Phys.* **2009**, *81*, 1827–1885.
- (36) Osawa, M.; Matsuda, N.; Yoshii, K.; Uchida, I. J. *Phys. Chem.* **1994**, *98*, 12702.
- (37) Griffith, W. P.; Koh, T. Y. *Spectrochim. Acta, Part A* **1995**, *51*, 253.
- (38) Le Ru, E. C.; Etchegoin, P. G. *Chem. Phys. Lett.* **2006**, *423*, 63–66.
- (39) Huang, F. M.; Baumberg, J. J. *Nano Lett.* **2010**, *10*, 1787–1792.